LETTERS

Three-dimensional atomic-scale structure of size-selected gold nanoclusters

Z. Y. Li[1], N. P. Young[1], M. Di Vece[1], S. Palomba[1], R. E. Palmer[1], A. L. Bleloch[3], B. C. Curley[2], R. L. Johnston[2], J. Jiang[4] & J. Yuan[4]

An unambiguous determination of the three-dimensional structure of nanoparticles is challenging[1]. Electron tomography requires a series of images taken for many different specimen orientations[2]. This approach is ideal for stable and stationary structures[3]. But ultrasmall nanoparticles are intrinsically structurally unstable and may interact with the incident electron beam[4–6], constraining the electron beam density that can be used and the duration of the observation. Here we use aberration-corrected scanning transmission electron microscopy[7], coupled with simple imaging simulation, to determine with atomic resolution the size, three-dimensional shape, orientation and atomic arrangement of size-selected gold nanoclusters that are preformed in the gas phase and soft-landed on an amorphous carbon substrate. The structures of gold nanoclusters containing 309±6 atoms can be identified with either Ino-decahedral, cuboctahedral or icosahedral geometries. Comparison with theoretical modelling of the system suggests that the structures are consistent with energetic considerations. The discovery that nanoscale gold particles function as active and selective catalysts for a variety of important chemical reactions has provoked much research interest in recent years[8–12]. We believe that the detailed structure information we provide will help to unravel the role of these nanoclusters in size- and structure-specific catalytic reactions[11,12]. We note that the technique will be of use in investigations of other supported ultrasmall metal cluster systems.

Scanning transmission electron microscopy (STEM), in the mode where incoherently scattered electrons are collected by a high-angle annular dark field (HAADF) detector, is appealing as a method of probing three-dimensional structure of nanoparticles (via an analysis of the intensity map from a single HAADF-STEM image) because its intensity is strongly dependent not only on the atomic number Z of the observed atoms but also on the number of atoms in a column[13,14].

The recent successful implementation of spherical aberration (C_s) correction in STEM[15] enables us to achieve the same analysis, but now at the atomic scale. We show that, by combining quantitative HAADF-STEM analysis with molecular-dynamics-based model structure search procedures and realistic image contrast simulations, it is possible to identify not only the size and shape but also the structure and orientation of soft-landed Au nanoclusters.

We demonstrate this for size-selected Au_N (where $N = 309 \pm 6$) clusters, where Au_{309} is known to be a possible 'magic number' nanocluster (see Supplementary Information). Figure 1a–c displays three high-resolution HAADF images taken from a Au_{309} nanoparticle. The images show outline shapes, which are approximately pentagonal, square and hexagonal, respectively. Close inspection of the intensity variation within the individual cluster images further reveals that the arrangement of the atomic columns varies from one cluster morphology to the other. Single Au atoms are also visible in the vicinity of the clusters or occasionally some distance away (two such atoms are marked by the circles in Fig. 1a and c). We have imaged the same clusters in several successive frames. The clusters sometimes move/rotate by small amounts and sometimes their structures change too. The individual atoms imaged on the carbon surface around the cluster also move from one frame to the next. The images shown in Fig. 1 are the first-pass images in each case.

To establish a foundation on which to analyse quantitatively the structure of the Au_{309} clusters, we carried out a series of integrated HAADF intensity measurements on size-selected Au clusters in the size range $N = 55$–$1,500$ atoms. For each sample, the HAADF intensity integrated over each cluster shows a narrow distribution (see Fig. 2 inset for $N = 309$). The mean intensity value taken for each cluster size is plotted as a function of the selected-size N in Fig. 2, where the standard deviation is used for estimating the error bars. The finite width of the distribution can be attributed partly to the
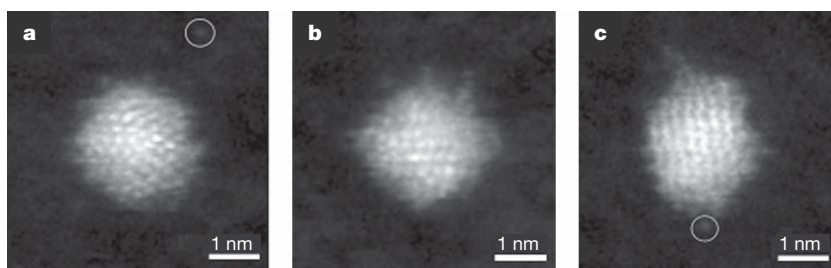
Figure 1 | High-resolution HAADF-STEM images of Au_{309} clusters on a carbon film. Typical images show various outline shapes, that is, cluster projections: pentagon (**a**), square (**b**) and hexagon (**c**). The intensity variation within the clusters clearly demonstrates atomic column resolution. Single atoms can be seen in the vicinity of the clusters, as indicated by the circle in **c**, and occasionally some distance away, as indicated by the circle in **a**. Resolution of the mass selector is ±2%.

[1]Nanoscale Physics Research Laboratory, School of Physics and Astronomy, [2]School of Chemistry, University of Birmingham, Birmingham B15 2TT, UK. [3]UK SuperSTEM Laboratory, Daresbury Laboratory, Daresbury WA4 4AD, UK. [4]Beijing Electron Microscopy Centre; Laboratory of Advanced Materials and Department of Materials Science and Engineering, Tsinghua University, Beijing 100084, China.
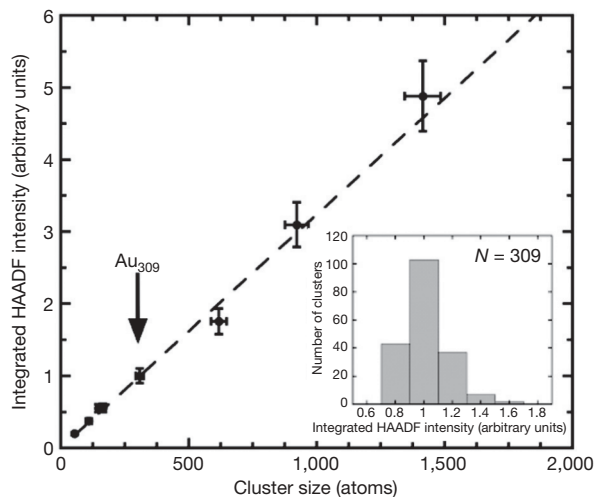
Figure 2 | Relationship between integrated HAADF intensity and size of gold clusters. Integrated HAADF intensity of size-selected Au clusters on amorphous carbon film plotted as a function of the number of atoms they contain, showing a linear relationship. The line is drawn as a guide to the eye. Each data point is obtained from a statistical intensity distribution analysis over a large number of clusters with a given number of atoms. The standard deviation is used for estimating the error bars. An example of such a distribution for Au_{309} is shown in the inset.

resolution of the mass-selector ($\pm 2\%$) and suggests that clusters soft-landing on the surface do not suffer significant fragmentation or coalescence. This is consistent with the results of our detailed image analysis, which reveals no extensive rafts of single atom layers on the amorphous carbon support, apart from a few 'shake-off' atoms. Figure 2 shows that the integrated HAADF intensity from the clusters increases linearly with the number of constituent atoms up to about $N = 1,500$. This linearity implies that, at small cluster size, atoms within the cluster contribute equally to the total scattered electron signal detected by the HAADF detector.

The linearity shown in Fig. 2 also suggests that the HAADF intensities for the individual atomic columns in Fig. 1 can be directly associated with the number of atoms in each column. The clear five-fold symmetry in the atomic column arrangement in Fig. 1a,

for example, suggests that the cluster has Ino-decahedral geometry and is oriented on the substrate such that the five-fold axis is parallel to the electron beam, as shown in the hard-sphere representation in Fig. 3a. Figure 3b displays an illustrative line intensity profile from the centre of this cluster to one of the corners, averaging over three experimental pixels (equal to 0.9 Å). Five peaks and a shoulder (marked by the arrow) are apparent, with the peak intensity decreasing gradually towards the corner. Using a simple kinematical approach, the simulated HAADF-STEM image of the decahedral Au_{309} cluster is shown in Fig. 3c, together with the intensity profile (the solid red curve). The correspondence between the simulated profile (Fig. 3c), and the experimental profile (Fig. 3b), with respect to both the peak positions and the relative peak intensities, is remarkable, indicating the correct identification of the atomic column structure. An icosahedron also has a five-fold rotational symmetry axis; however, the rotation-reflection symmetry of this structure results in a STEM image having ten-fold symmetry, and the technique described has the potential to discriminate between these two possible structures (see Supplementary Information). We have also conducted a full dynamical calculation using the multislice method[16]. The corresponding line profile is shown by the dashed line in Fig. 3c. The similarity between the two simulated line profiles confirms the validity of the simple kinematical approximation for HAADF-STEM image simulation of the Au_{309} clusters and that the quantization of the HAADF intensity correlates directly with the quantization of the number of the atoms.

Close comparison between Fig. 3b and c also highlights a discrepancy in the atom columns at the edge of the cluster. The experimental intensity of the outermost atomic column is significantly lower than those predicted by either simulation. In addition, an extra shoulder appears in the experimental profile, as indicated by the arrow, with a peak intensity lower than that of the isolated single Au atom observed on the same sample (Fig. 1a). This shoulder exists for all the clusters inspected, irrespective of their shape. The discrepancy cannot be wholly explained by effects such as the rocking movement of the cluster under the electron beam, electron-beam scan instability or noise from other sources, because all these effects would result in the smearing out of the overall image. We take it as evidence that atoms in the surface layer of the clusters fluctuate significantly, on a time-scale shorter than the period for the data acquisition. This is similar
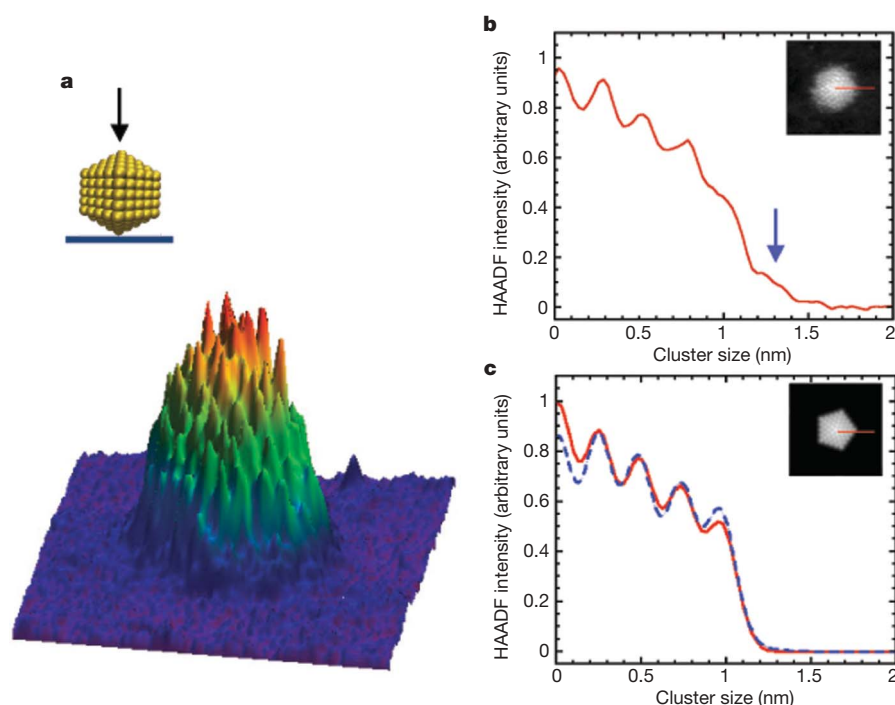
Figure 3 | Three-dimensional atomic structure of a gold cluster ($N = 309 \pm 6$). a, Three-dimensional atom density profile of Au_{309}, derived from Fig. 1a. A hard-sphere model for an Ino-decahedral structure is shown with the electron beam (arrow) parallel to the five-fold axis. **b,** Experimental intensity line profile taken from the central atom column of the cluster to one of the corners (indicated in inset with red line). **c,** Simulated HAADF-STEM image (inset), obtained with a simple kinematical approach, of an Au_{309} cluster with Ino-decahedral geometry. An intensity profile (solid curve) across one ridge (indicated in inset with red line) is compared with the result from a full dynamical multislice calculation (dashed line).

to the dynamic motion of surface atoms previously observed for larger nanoparticles[17,18].

The observed structures of the Au clusters can be understood from their calculated total potential energies for different polyhedral geometries (icosahedral, Ino-decahedral and cuboctahedral) as a function of the number of constituent atoms. After local energy minimization, it was found that, for very small Au clusters ($N < 100$), the icosahedral structure is much more stable than the Ino-decahedral and the cuboctahedral structures. The total potential energy is in the order of: icosahedral < Ino-decahedral < cuboctahedral. However, for the larger clusters ($N \approx 500$–$1,000$), the order of stability begins to change, with the Ino-decahedral structure becoming more stable than the icosahedral geometry: Ino-decahedral < icosahedral < cuboctahedral. Further increasing the cluster size results in the order of stability changing to: Ino-decahedral < cuboctahedral < icosahedral. For Au_{309}, the difference in total energy between different geometries was less than 1.2 eV (that is, less than 3.88 meV per atom) from the most stable to the least stable. Moreover, there are many local energy minima and the energy barriers between these structures are small. These results support our experimental findings that no one structure dominates. For Au_{309}, we see a similar proportion of clusters with Ino-decahedral (32%) and cuboctahedral (25%) structures and a much lower population of icosahedral structures (8%). In the remaining population, some clusters show irregular facets and some do not show any ordered geometry, possibly because of significant rearrangement of the outer-shell atoms, akin to the solid–liquid phase coexistence predicted for other systems[19]. Given the narrow size distribution of the deposited clusters, our results may shed light on the relative structural stabilities of the various cluster isomers in the gas phase, information that has solicited many theoretical investigations but little hard experimental evidence.

In conclusion, we have demonstrated the suitability of high-angle annular dark-field imaging in the aberration-corrected STEM for detailed structural and stability analysis of size-selected metallic clusters on solid supports at atomic resolution. The multiplicity of cluster geometries revealed by our detailed study of the atomic arrangement of soft-landed Au_{309} clusters on amorphous carbon supports is consistent with many local energy minima predicted for clusters of this size by cluster simulations. Evidence for increased fluctuations and motion of cluster surface atoms relative to the core atoms within the Au_{309} clusters may reflect an inherent property of the nanometre-sized gold clusters that could be related to their enhanced catalytic properties through much reduced coordination. Vertical depth information can be extracted from a single projection, with single-atom sensitivity, opening up the possibility to use the technique as a routine three-dimensional structural characterization tool for small nanoparticles at the atomic-scale level, with the help of image simulation based on *ab initio* cluster modelling including dynamical effects. The experimental approach has practical advantages, such as the more relaxed constraints on cluster stability[17,18]. When combined with time-lapsed imaging techniques, our approach could provide the dynamical insight into the atomistic structural changes of nanoparticles that commonly occur in some catalytic reactions[20].

METHODS SUMMARY

The gold clusters are formed by gas-phase condensation of sputtered atoms in a rare-gas atmosphere[21], size-selected by a lateral time-of-flight mass spectrometer[22] and soft-landed on an amorphous carbon support[23] for examination by high-angle annular dark-field STEM, using a spherical-aberration-corrected machine for the atomically resolved imaging[24]. The three-dimensional atomic structures of the size-selected clusters are obtained by comparison of the experimental results with both kinematic and dynamical image simulations[16,25], based on structural models optimized by a realistic many-body potential[26,27].

1. Koga, K., Ikeshoji, T. & Sugawara, K. Size- and temperature-dependent structural transitions in gold nanoparticles. *Phys. Rev. Lett.* **92**, 115504–115507 (2004).
2. Midgley, P. A. & Weyland, M. 3D electron microscopy in the physical sciences: the development of Z-contrast and EFTEM tomography. *Ultramicroscopy* **96**, 413–431 (2003).
3. Arslan, I., Yates, T. J. V., Browning, N. D. & Midgley, P. A. Embedded nanostructures revealed in three dimensions. *Science* **309**, 2195–2198 (2005).
4. Iijima, S. & Ichihashi, T. Structural instability of ultrafine particles of metals. *Phys. Rev. Lett.* **56**, 616–619 (1986).
5. Ajayan, P. M. & Marks, L. D. Experimental evidence for quasimelting in small particles. *Phys. Rev. Lett.* **63**, 279–282 (1989).
6. Marks, L. D. Experimental studies of small particles structures. *Rep. Prog. Phys.* **57**, 603–649 (1994).
7. Batson, P. E., Dellby, N. & Krivanek, O. L. Sub-angstrom resolution using aberration corrected electron optics. *Nature* **418**, 617–620 (2002).
8. Haruta, M. Size- and support-dependency in the catalysis of gold. *Catal. Today* **36**, 153–166 (1997).
9. Sanchez, A. *et al.* When gold is not noble: nanoscale gold catalysts. *J. Phys. Chem. A* **103**, 9573–9578 (1999).
10. Hughes, M. D. *et al.* Tunable gold catalysts for selective hydrocarbon oxidation under mild conditions. *Nature* **437**, 1132–1135 (2005).
11. Tsunoyama, H., Sakurai, H., Negishi, Y. & Tsukuda, T. Size-specific catalytic activity of polymer-stabilized gold nanoclusters for aerobic alcohol oxidation in water. *J. Am. Chem. Soc.* **127**, 9374–9375 (2005).
12. Chen, M. S. & Goodman, D. W. Structure-activity relationships in supported Au catalysts. *Catal. Today* **111**, 22–33 (2006).
13. Li, Z. Y., Yuan, J., Chen, Y., Palmer, R. E. & Wilcoxon, J. P. Direct imaging of core-shell structure in silver-gold bimetallic nanoparticles. *Appl. Phys. Lett.* **87**, 243103 (2005).
14. Li, Z. Y., Yuan, J., Chen, Y., Palmer, R. E. & Wilcoxon, J. P. Local three-dimensional visualization of nanoparticle assemblies. *Adv. Mater.* **17**, 2885–2888 (2005).
15. Krivanek, O. L., Delby, N. & Lupini, A. R. Towards sub-angstrom electron beams. *Ultramicroscopy* **78**, 1–11 (1999).
16. Kirkland, E. J. *Advanced Computing in Electron Microscopy* (Plenum Press, New York/London, 1998).
17. Smith, D. J., Petford-Long, A. K., Wallenberg, L. R. & Bovin, J.-O. Dynamic atomic-level rearrangements in small gold particles. *Science* **233**, 872–875 (1986).
18. Bovin, J.-O., Wallenberg, R. & Smith, D. J. Imaging of atomic clouds outside the surfaces of gold crystals by electron microscopy. *Nature* **317**, 47–49 (1985).
19. Schebarchov, D. & Hendy, S. C. Transition from icosahedral to decahedral structure in a coexisting solid-liquid nickel cluster. *Phys. Rev. Lett.* **95**, 116101–116104 (2005).
20. Hansen, P. L. *et al.* Atom-resolved imaging of dynamic shape changes in supported copper nanocrystals. *Science* **295**, 2053–2055 (2003).
21. Pratontep, S., Carroll, S. J., Xirouchaki, C., Streun, M. & Palmer, R. E. Size-selected cluster beam source based on radio frequency magnetron plasma sputtering and gas condensation. *Rev. Sci. Instrum.* **76**, 045103–045109 (2005).
22. von Issendorff, B. & Palmer, R. E. A new high transmission infinite range mass selector for cluster and nanoparticle beams. *Rev. Sci. Instrum.* **70**, 4497–4501 (1999).
23. Palmer, R. E., Pratontep, S. & Boyen, H.-G. Nanostructured surfaces from size-selected clusters. *Nature Mater.* **2**, 443–448 (2003).
24. Bleloch, A. L. & Lupini, A. Imaging at the picoscale. *Mater. Today* **7**, 42–48 (2004).
25. Jiang, J., Yuan, J. & Bleloch, A. L. Cluster-scale composition determination in a boron-rich compound. *Appl. Phys. Lett.* **91**, 113107 (2007).
26. Cleri, F. & Rosato, V. Tight-binding potentials for transition metals and alloys. *Phys. Rev. B* **48**, 22–33 (1993).
27. Johnston, R. L. Evolving better nanoparticles: Genetic algorithms for optimising cluster geometries. *Dalton Trans.* 4193–4207 (2003).

METHODS

Cluster formation and deposition. Gold cluster beams were produced by a source based on radio-frequency magnetron plasma sputtering and gas aggregation[21]. The positively ionized clusters were extracted and focused by ion optics and mass-selected (resolution, ±2%) by a lateral time-of-flight mass filter[22]. The clusters were deposited on a transmission electron microscope grid coated with an amorphous carbon film with a deposition energy of 500 eV, which is in the soft-landing regime, to ensure the maximum probability of retaining the pre-formed cluster structure upon deposition[23].

Electron microscope imaging. Systematic measurements of integrated HAADF intensities for a wide range of size-selected Au clusters were carried out using a Tecnai F20 200 kV STEM at the Nanoscale Physics Research Laboratory, University of Birmingham. High-resolution imaging of Au_{309} clusters was performed using a dedicated VG HB501 STEM at the UK SuperSTEM facility at Daresbury[24]. This was fitted with a second-generation spherical-aberration corrector from Nion Inc. and operated at 100 kV. These images were captured by a high-angle annular dark-field detector with a probe convergence angle of 24 mrad and collection angle from 70 to 200 mrad. The beam current was typically 70 pA. All images were recorded at a rate of 19 μs per pixel. The images in Fig. 1 were extracted from a $1,024 \times 1,024$ pixel image and are 170×170 pixels. They have been low-pass filtered (with a 3×3 kernel and a weight of 1.2) using the SPIP program (version 3.2.0.1, Image Metrology).

Structure modelling. To simulate HAADF images of the Au_{309} clusters for comparison with experiments, we first generated idealized icosahedral, Ino-dechedral and cuboctahedral geometries with the magic number $N = 309$. The structures, which were modelled by the Gupta many-body potential[26] for Au, were then locally relaxed. This was followed by a detailed genetic algorithm search[27] for Au_{309} cluster structures.

Kinematical STEM simulation. This was done by locating each trial cluster within a two-dimensional grid of dimensions $50\,\text{Å} \times 50\,\text{Å}$, with an interval spacing of $0.25\,\text{Å}$ in both the x and y coordinates. A probe of diameter $1\,\text{Å}$ visited each grid point and checked for atoms within the probe radius of this grid point in the two-dimensional x–y plane. The quantitative contribution of an atom to the intensity was related to the actual distance between the probe centre and the centre of the atom by a gaussian distribution. All the atomic contributions within the probe radius were then summed and used to calculate the total intensity. Finally, we examined the calculated image for various alignments of each cluster relative to the electron beam probe. The above procedure was repeated for high-symmetry clusters with the magic number $N = 309$, including the icosahedron, the cuboctahedron and the Ino-decahedron structures.

Multislice STEM simulation. We have used an approach described by Kirkland[16] that allows the atomic potential at each layer to be different. Therefore, the image of a particle can be calculated by putting the appropriate number of atoms in each layer of the multislice calculation in accordance with the cluster geometry. To simulate the HAADF image of the cluster, a supercell was built by putting a single cluster into a box of dimension $60 \times 60 \times 25\,\text{Å}^3$. The same relaxed atomic coordinates as in the kinematical simulation were used for the Au_{309} clusters. In the beam direction, the sample is sliced into 17 layers. The sampling is $1,024 \times 1,024$ for the supercell and this configuration covers the scattering angle up to about 210 mrad. The frozen phonon method was used to include the thermal diffuse scattering with a constant Debye–Waller factor of $0.0057\,\text{nm}^2$. The experimental probe parameters we used were $C_5 = 70$ mm, $C_3 = -0.026$ mm and $C_1 = 5$ nm with convergence angle aperture of 24 mrad. The resulting probe profile has a full-width at half-maximum (FWHM) of about 0.08 nm. The scattering factor for gold was taken from ref. 16.